3

Low-energy Ion Outflow Observed by Cluster: Utilizing the Spacecraft Potential

S. Haaland[1,2], M. André[3], A. Eriksson[3], K. Li[2], H. Nilsson[4], L. Baddeley[5], C. Johnsen[6], L. Maes[7], B. Lybekk[8], and A. Pedersen[8]

Video of Yosemite Talk, URL: http://dx.doi.org/10.15142/T3MS30

ABSTRACT

A significant amount of mass is lost from the Earth's atmosphere through ions escaping from the polar ionosphere. Due to spacecraft charging effects, in situ measurements using traditional plasma instruments are typically not able to detect the low energy part of the outflow. Recent advances in instrumentation and methodology, combined with comprehensive data sets from the Cluster constellation of spacecraft have provided far better opportunities to assess the role of the low energy ions. With this new technique, it is possible to bypass detection problems caused by spacecraft charging effects, and provide quantitative, in situ estimates of cold ion density and outflow velocity. In this chapter, we give an overview of these advances and highlight some of the key results based on this methodology. The results corroborate earlier findings that polar rain and the open polar cap is the primary source of cold outflow, but we also find enhanced cold outflow from the cusp and auroral zone though, in particular during disturbed geomagnetic conditions. The transport of cold ions is mainly governed by the convection, and most of the outflowing ions are transported to the nightside plasma sheet and recirculated in the magnetosphere. Transport times are of the order of two to four hours from the ionosphere to the nightside magnetospheric plasma sheet. Direct loss along open field lines downtail into the solar wind only takes place during quiet magnetospheric conditions with low or stagnant convection. Only about 10% of the total cold outflow is directly lost downtail into the solar wind.

[1]*Birkeland Centre for Space Science, University of Bergen, Norway*

[2]*Max-Planck Institute for Solar Systems Research, Göttingen, Germany*

[3]*Swedish Institute of Space Physics, Uppsala, Sweden*

[4]*Swedish Institute of Space Physics, Kiruna, Sweden*

[5]*Birkeland Centre for Space Science, The University Centre in Svalbard, Longyearbyen, Norway*

[6]*Department of Geophysics, University of Oslo, Norway*

[7]*Royal Belgian Institute for Space Aeronomy, Brussels, Belgium*

[8]*Department of Physics, University of Oslo, Norway*

3.1. INTRODUCTION

Every day, the Earth loses a significant amount of mass through escape of atmospheric material into space. Much of the loss is made up by ionized material, and the outflow of low energy ions of ionospheric origin is believed to be a significant contributor to the magnetospheric plasma population [*Horwitz*, 1982; *Chappell et al.*, 1987; *André and Cully*, 2012].

Escape from the atmosphere, whether neutral or ionized, can be understood by considering the forces acting

Magnetosphere-Ionosphere Coupling in the Solar System, Geophysical Monograph 222, First Edition.
Edited by Charles R. Chappell, Robert W. Schunk, Peter M. Banks, James L. Burch, and Richard M. Thorne.

on the thermospheric constituents. If the total upward forces exceed downward forces, ions are accelerated upward and can potentially escape. Gravity is usually the main downward force and acts on both neutrals and ions, and depends on mass and altitude. For neutrals, pressure gradients due to thermal effects constitute the dominant upward force. For ions, the picture is more complicated, and additional electromagnetic forces must be taken into account. Some of these forces (which may be directed either upward or downward) depend on the mass of the particle; others do not. Charge (and charge state) also play a role for electromagnetic forces.

It is often convenient to cast the force balance picture into an energy balance analogy. In this description, the Earth's gravitational potential energy balanced against the ions' upward directed kinetic energy. For particles at rest, minimum escape energies for protons and oxygen from the Earth are around 0.6 and 10 electron-volt (eV), respectively.

Above the open polar cap regions, where no hydrostatic equilibrium can be established, low energy electrons, due to their low mass, can easily escape the Earth's gravitational potential [e.g., *Dessler and Michel*, 1966]. As a consequence, an ambipolar electric field arises due to the charge separation. This ambient electric field acts as a force on charged particles and decelerates electrons and accelerates ions [see e.g., *Kitamura et al.*, 2017, (this volume) and references therein for more details here]. Simulations by *Su* [1998] suggest a resulting total potential drop on the order of a few 10s of volts over an altitude of several Earth radii (R_E 6371 kilometer [km]). This ambient electric field, although very small, is sufficient to maintain a flow of plasma from the ionosphere into the magnetosphere. This outflow, the polar wind, was first predicted by models [*Axford*, 1968; *Banks and Holzer*, 1968]. Experimental observations of the polar wind from were first reported by *Hoffman* [1970] and later in other sources [e.g., *Hoffman et al.*, 1974; *Chandler et al.*, 1991; and *Abe et al.*, 1993]. See also *Yau et al.* [2017] (this volume) for a comprehensive overview. All these observations were taken below 1 R_E altitude.

At higher altitudes (above a few R_E), it becomes notoriously difficult to measure the low energy part of the outflowing plasma population. In the tenuous plasma polar cap and lobe regions of the Earth's magnetosphere, the spacecraft voltage often reaches several tens of volts positive due to photo emissions. This spacecraft potential will shield low energy ions from reaching the spacecraft sensors. Unless the effects of spacecraft charging can be eliminated, cold ions therefore remain invisible for particle detectors. Attempts to bypass this problem has so far typically involved some form of active spacecraft potential control. A notable example utilizing this kind of neutralization is the study by *Su et al.* [1998], which used particle measurements from the Polar spacecraft. During a limited time period the onboard Plasma Source Instrument (PSI) was operating, and was able to keep the spacecraft voltage at a few volts. *Su et al.* [1988] were then able to observe and characterize polar wind outflow at high altitudes.

The Cluster spacecraft [*Escoubet et al.*, 1997; *Escoubet and Schmidt*, 2000], forming the basis for most of the results discussed in the present paper, also has an active spacecraft potential control [Active Spacecraft Potential Control (ASPOC), see *Riedler et al.*, 1997] but to our knowledge no specific study focusing on polar wind or ion outflow has systematically utilized this. Furthermore, active spacecraft control typically works by emitting metallic ions from a finite reservoir. Continuous operation over an extended time is therefore not feasible. The last ASPOC instrument on Cluster ceased working in 2006 when this reservoir was depleted [*Torkar and Jeszenszky*, 2010].

Engwall et al. [2006] presented a completely different approach to cold ion outflow detection. By utilizing data from two independent electric field instruments, they were able to exploit spacecraft charging to derive densities and outflow velocities of cold plasma. Basically, a supersonic flow of low-energy ions forms a wake behind the charged spacecraft. The electric field caused by this wake, combined with a functional dependence between the ambient plasma density and the spacecraft potential, is then used to determine the cold ion outflow. This technique has been applied by a number of follow-up studies, e.g., *Engwall, et al.* [2009a]; *Nilsson et al.* [2010]; *Haaland, et al.* [2012a, b]; *Li et al.* [2012, 2013]; *André et al.* [2014]; *Haaland et al.* [2015]; *Li et al.* [2016].

The purpose of this chapter is to give an overview of the methodology and some of the key results obtained from this new technique. The chapter is organized as follows: In Section 2, we explain why cold ion measurements are difficult and how the instrumentation onboard Cluster is used to bypass these difficulties. Thereafter, in Section 3, we present a description of the Cluster cold ion data set and its characteristics. Section 4 presents some of the results based on this methodology. Finally, Section 5 is a summary of the results.

3.2. THE COLD ION DETECTION CHALLENGE

So why are measurements of cold ion so difficult, and why are low energy ions sometimes referred to as *invisible* or *hidden* [e.g., *Olsen*, 1982; *Olsen et al.*, 1985; *Chappel et al.*, 1987, 2000; *André and Cully*, 2012]? To answer these question, we have to take a closer look at the environment in which spacecraft operate.

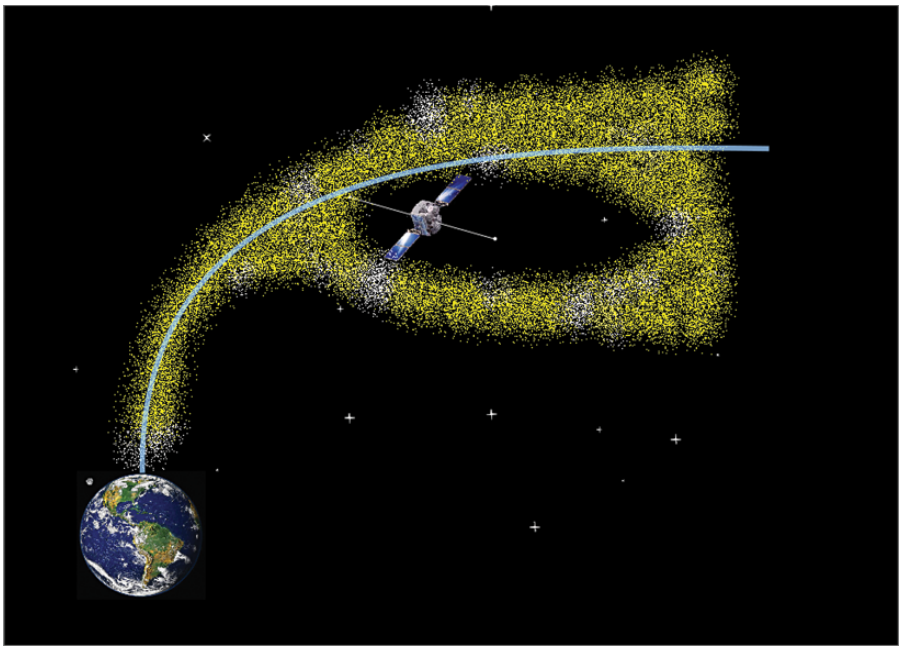

Figure 3.1 Illustration of shielding due to spacecraft charging. Low energy ions emanating from the polar cap region travel upward along the magnetic field lines. Due to a positive spacecraft charge, ions with energies below the spacecraft potential energy will not reach particle detectors onboard the satellite; they remain 'invisible.' A wake, void of ions, but filled with electrons, will be formed downstream of the spacecraft.

Spacecraft traversing the high altitude polar cap and the magnetically connected lobe regions spend most of their time in sunlight. Solar radiation, in particular the ultraviolet (UV) and extreme ultraviolet (EUV) range, corresponding to 2 to 20 nanometer (nm) wavelengths, causes photoelectron emissions from the surface of the spacecraft. In low density plasma regions like the high altitude polar cap regions and in the magnetotail lobes, this electron loss cannot be compensated. The result is a current imbalance, with a net electron current away from the spacecraft. In the lobe and polar cap, where the tenuous plasma is insufficient to replenish the electron loss, the spacecraft will end up with an excess of positive charges. Consequently, the spacecraft can end positively charged to several 10s of volts [see e.g., *Lybekk et al.*, 2012]. Unless this charging can be prevented or circumvented, this will cause problems for low energy plasma measurements.

Typically, there are no strong heating or field aligned acceleration mechanisms above the polar cap region or in the lobes, and the outflowing ions will not gain significant energy as they move outward. Ions of ionospheric origin are therefore characterized (and identified) by low energies. If the energy of the ions is below the spacecraft potential energy (eV_{SC}, where e is elementary charge and V_{SC} is the spacecraft charge relative to the ambient plasma), these ions will be deflected away from the positively charged spacecraft. Unless the ions have sufficient energy to overcome this deflection, they will not be able to reach particle detectors on the spacecraft. They are "invisible" as illustrated in Figure 3.1.

In the following, we will refer to these ions as "cold," where the term cold implies that the total energy of the ions is below the spacecraft potential energy. Note that this inability to measure cold ions is completely independent of particle sensor properties such as sensitivity, noise levels, and energy thresholds. Spacecraft charging implies that the particles to be measured simply do not reach the sensors. A completely different approach is therefore required.

Remote sensing of cold ion outflow is also difficult. Ground-based measurements (e.g., incoherent scatter radars) can only measure up to about 1000 km altitude. Vertical upward motion at these altitudes, sometimes termed upwelling, is is often associated with a significant downward vertical motion. It is thus difficult to assess how much plasma actually reaches escape velocity and eventually escapes the Earth's gravitational field. Given that the ambipolar electric field responsible for the escape can span several Earth radii in altitude, low orbit satellites, although often less affected by spacecraft charging due to higher ambient plasma densities, have similar issues.

3.2.1. Utilizing Spacecraft Potential and Wake

A unique feature of the Cluster satellite mission is the combination of two complementary electric field experiments, the Electron Drift Instrument (EDI) [see

Paschmann et al., 1997; *Quinn et al.*, 2001] and the Electric Field and Wave (EFW) experiment [see *Gustafsson et al.*, 2001]. This combination is the key element for the new technique to estimate cold ion flux.

EFW is a classic double probe experiment, consisting of two pairs of equally shaped spherical probes, each mounted on a wire boom approximately 40 meters (m) away from the spacecraft body. Only the spin plane electric field can be measured by EFW, but by assuming no or negligible electric potential drop along the magnetic field, $E_{\perp} >> E_{\parallel}$, the full three-dimensional electric field can sometimes be estimated.

EDI is based on the drift of an electron gyro center in the presence of external forces. Each Cluster spacecraft is equipped with two EDI gun/detector units. Each gun emits a modulated electron beam with a fixed beam energy. The beam energy can be switched between 500 eV and 1 keV to measure the effects of magnetic gradients, but because these are usually small compared to the local electron gyro radius, the beam is typically kept fixed at 1 keV. The direction of this beam is continuously controlled through a servo loop so that the beam returns to the detector unit. The gyro center position and motion can then be determined from triangulation (or, in some regions, from the time of flight of the emitted electrons). For a known magnetic field with negligible gradients, the gyro center drift of the emitted beam is proportional to the convective electric field. The measurement principle of EDI does not allow for a continuous operation in all plasma regimes, but in regions with fairly stable magnetic field, and low electron background plasma, EDI provides the full three-dimensional convective electric field with very high accuracy.

3.2.1.1. Cold Plasma Density

The spacecraft charge can be used to our advantage, however. Regarding spacecraft charge, the voltage difference between the probes is assumed to be at or close to the ambient plasma potential and the electric potential of the spacecraft body.

Spacecraft charging depends on solar irradiance, spacecraft surface material, spacecraft surface area, and the ambient plasma density. With the former parameters known, it is possible to use the spacecraft potential to estimate the ambient electron density, and thus the plasma density [e.g., *Pedersen et al.*, 2001, and references therein]. In general, a relation of the form

$$N_e = Ae^{-BV_{SC}} + Ce^{-DV_{SC}} \tag{3.1}$$

exists. N_e is the sought after electron density, V_{SC} is the spacecraft potential relative to the ambient plasma. The coefficients A, B, C, and D are determined from calibrations against other measurements, and implicitly contain information about solar illumination and spacecraft surface properties. In *Lybekk et al.* [2012], the charge effect caused by the EDI electron emission was also taken into account and incorporated into the above calibration coefficients.

3.2.1.2. Cold Ion Bulk Velocity

The bulk flow of the plasma can be obtained by combining measurements from the EDI and EFW instruments onboard Cluster.

If the bulk energy, E_{Ki} of the cold ions flowing across the spacecraft is larger than their thermal energy, kT_i, i.e., the following inequality exists:

$$kT_i < E_{Ki} < eV_{SC}, \tag{3.2}$$

a wake void of ions will be formed downstream of the spacecraft. Electrons, however, with their higher mobility (typically $kT_e >> E_{Ke}$), will be able to fill the wake. Consequently, an electric field, $\vec{E}^W$ along the bulk flow direction, $\vec{u}$ will arise:

$$\vec{E}^W = g\vec{u} \tag{3.3}$$

where the scaling factor, g, is a function of the local plasma parameters, and can be experimentally determined [*Engwall et al.*, 2006].

The size of the wake is comparable to the boom-to-boom scale size of the spacecraft but much smaller than the gyro radius of the 1 keV electron beam emitted by EDI. Thus, EFW will be influenced by the artificial electric field, whereas EDI is not affected. The wake electric field can therefore expressed as a deviation between the electric field measured by EFW, $\vec{E}^{EFW}$ and the real, unperturbed ambient electric field $\vec{E}^{EDI}$

$$\vec{E}^W = \vec{E}^{EFW} - \vec{E}^{EDI} = g\vec{u} \tag{3.4}$$

Note that the perpendicular part of the bulk flow, $\vec{u}_{\perp}$, is obtained directly from the EDI measurements; $\vec{u}_{\perp} = \vec{E}^{EDI} \times \vec{B}/B^2$. The parallel component of u is then obtained by first decomposition $\vec{E}^W$ into two spin plane component, E_x^W and E_x^W. An explicit expression for the parallel bulk velocity of the cold ions is thereafter obtained from:

$$u_{\parallel} = \frac{E_x^W u_{\perp}, y + -E_y^W u_{\perp}, x}{E_y^W B_x - E_x^W By} \tag{3.5}$$

where B is the magnetic field.

Note that wake formation as such is not exclusive to the polar cap or lobe regions [e.g., *Whipple et al.*, 1974 and references therein], but the combination of the two electric field measurements onboard Cluster has made determination of the bulk velocity possible for the first time.

3.2.1.3. Flux of Cold Ions

From the above equations (1) and (5), the flux of cold ions at the spacecraft position can now be determined:

$$f_{\parallel} = N_e * u_{\parallel} \tag{3.6}$$

We shall refer to the above $f_{\parallel}$ as local flux, noting that it is the in situ flux at Cluster, taken anywhere between 4 and 19 R_E altitudes. To facilitate comparison with other ion outflow measurements, and to estimate the total outflow, it is useful to normalize the outflow to a certain altitude, typically the topside ionosphere or exobase. Using flux conservation considerations and magnetic flux tube cross section from a magnetic field model, we can now scale this flux to ionospheric altitudes (here 1000 km). We shall later refer to this as *mapped flux*. The total outflow can then be obtained by integrating this mapped flux over the source area.

3.2.2. Estimating Total Outflow Rates

In the outflow estimates given in *Engwall et al*. [2009a, 2009b], it was assumed that the source area was the open polar cap region, simply defined as the area above 70° invariant latitude at 1000 km altitude. They also made no provisions for any time dependent or disturbance dependent variations of the total polar cap area, and also assumed identical areas in the Northern and Southern Hemisphere. *Haaland et al*. [2012a, 2012b], used a slightly more realistic approach based on a model by *Storelis et al*. [1998], which took into account variation in polar cap size. Later, *Li et al.* [2012], using the same data set, confirmed that the open polar cap was the source region. These results also demonstrated large variation in the source area with disturbance levels; the source area was significantly larger during disturbed conditions, consistent with an expanding and contraction polar cap.

3.2.3. Constraints and Limitations in Data and Method

It is fair to say that the above methodology and the Cluster cold ion data set can only provide a partial view of the total escape of ionized material from the Earth's atmosphere.

From the above derivation, one notes that it is not possible to distinguish between different ion species. Nor is any distinction between ion charge state possible. The wake method is more sensitive to lighter ions, as these are more affected by the wake, however. Observations by *Su et al.* [1998] indicate that hydrogen is the dominant species in low-energy outflow from the polar cap region. Nevertheless, in *Engwall et al.* [2009a] and *André et al.* [2014] the derived densities were lowered by a factor of 0.8 to account for the presence of heavy ions. In reality, the abundance of heavier ions, typically oxygen, varies both with geomagnetic activity and source location. Oxygen is more likely to emanate from the cusp and auroral zone [e.g., *Yau and Andre*, 1997; *Lockwood et al.*, 1985a, 1985b], though.

Equation (2) puts limits on temperature and bulk energy of the ions possible to detect. Also, since the velocity determination rests on the identification of a downstream wake (which is not always observed, even in the polar cap and lobe regions), the data set is not continuous in time. The bulk flow direction should have a significant component along the spin plane of the spacecraft. Otherwise, the EFW probes will not be able to measure the wake field. This is usually no issue in the lobes, where the magnetic field is stretched out, but can be an issue closer to Earth.

Also, as with any collection of experimental data, there are uncertainties related to both measurements, methodology, and the underlying assumptions. *Engwall et al.* [2009a] estimated that error due to methodology is of the order of ± 40% or less for velocity calculations and of the order of 20% for electron density calculations. The statistical spread in the observations is much larger than this.

3.3. THE CLUSTER COLD ION DATA SET

Cluster consists of four identical spacecraft flying in formation with varying separation distance. The orbit is an approximately 4 x 19 R_E polar orbit with a duration of about 57 hours. The spacecraft traverses the lobe region from July to October, so the cold ion observations are limited to this season. In the community, the four spacecraft are conveniently referred to as C1, C2, C3, and C4. The instrumentation is identical, but not all instruments work on all spacecraft. In particular, EDI data are available from C1 and C3 throughout the time period 2001 to 2010 relevant for the present paper. EDI data from C2 are available until early 2004 but has not been used to derive cold ion data. No EDI data are available from C4. Data from EFW are available from all four spacecraft, with limitations as described in *André et al*. [2014]. In particular, EFW data from C3 are less useful during much of 2006 due to mismatch between instrument bias current settings and actual photoemissions.

Two large data sets based on Cluster observations and the above wake method have been compiled. The first data set, derived and presented in *Engwall et al*. [2009a], consists of approximately 170,000 records with cold ion density and bulk outflow velocity. This data set is based on C3 measurements for the years 2001 to 2005.

In 2013, the EFW team in Uppsala started a project to update and extend the Cluster cold ion data set. This involved analysis also of data from the Cluster C1 spacecraft, and also for later years. This new data set presently

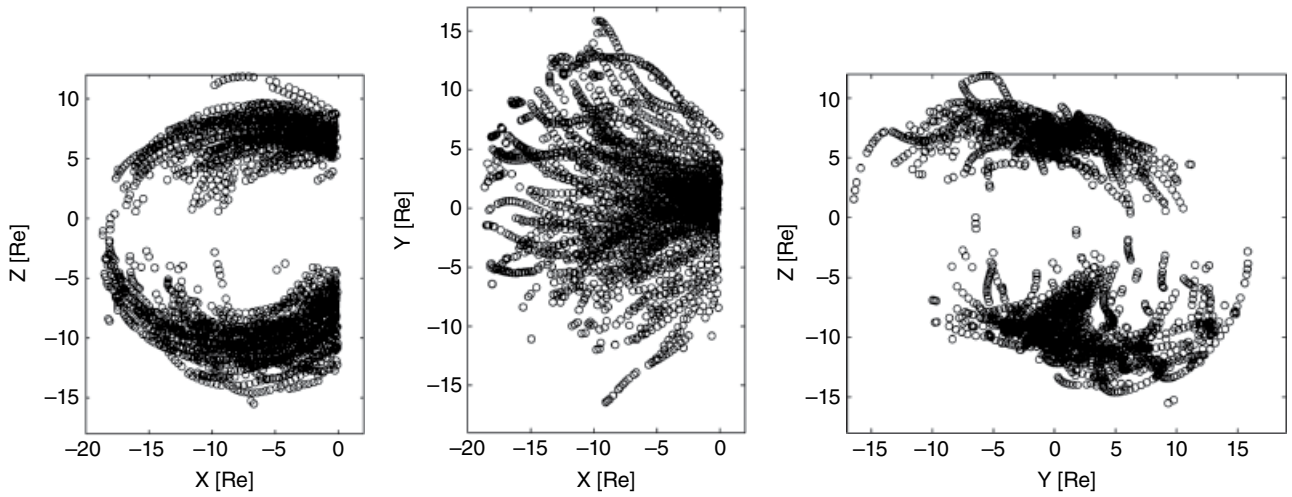

Figure 3.2 Illustration of data coverage for the current Cluster cold ion data set. Each black dot represents the position of an individual wake detection from which the flux could be determined. From left to right, the coverage as projected into the XZ_{GSM}, XY_{GSM}, and ZY_{GSM} planes, respectively.

consists of data from C1 and C3 for 2001 to 2010, although the lower solar activity means that there are less data from later years. In total, this dataset contains approximately 320,000 records from which reliable cold ion fluxes could be determined. Details and characteristics of this data can be found in *André et al.* [2014]. The spatial coverage for this combined set, illustrated in Figure 3.2, is similar to the earlier data set, but the larger number of records and the extended time interval opens for new studies, e.g., effects of solar cycle variations.

3.4. RESULTS

In the following section, we highlight some of the main results based on Cluster measurements of cold ions. At the time of writing (2015), the extended cold data set and the publication by *André et al.* [2014] had just been released. With a few exceptions, most of the results discussed below are therefore based on the original cold ion dataset as described in *Engwall et al.* [2009a].

3.4.1. Characteristic Cold Ion Densities and Velocities

Initial cold ion outflow rates were established by *Engwall et al.* [2009a] and found to be comparable to earlier estimates based on particle instruments (and thus higher energies). Integrated over the whole polar cap, outflow rates of the order of 10^{26} ions/s were reported. *André et al.* [2014] obtained similar rates using the extended data set. In large parts of geospace, for example the lobe regions, little or no heating or acceleration takes place, and cold ions seem to dominate the plasma population [*André and Cully*, 2012].

Figure 3.3 shows the distribution of measured outflow velocities (panel a) and densities (panel b) but is based on the full data set prepared by *André et al.* [2014]. We have removed records with negative velocities, because these suggest motion into the ionosphere. Values shown are taken from both hemispheres.

The locally measured mean and median densities of the full data set (i.e., no subsetting according geomagnetic activity, solar activity, or similar) are 0.21 and 0.13 centimeter $(cm)^{-3}$, respectively. Mean and median outflow velocities are 27 and 23 km/s^{-1}, respectively, once again based on the full data set. Panel c of Figure 3.3 shows the velocity and density as a function of altitude. Each point in this panel represents the average (mean) velocity within the given altitude range. Velocities increase with increasing radial distance, indicating acceleration, presumably due to centrifugal forces [*Cladis*, 1986; *Nilsson et al.*, 2010]. Densities decrease with radial distance as expected from the expanding flux tubes.

3.4.2. Identifying the Source Region

As mentioned above, the fundamental cause of the polar wind is the lack of hydrostatic equilibrium above the open polar cap, which causes escape of electrons and consequently an ambipolar electric field that extracts low energy ions. In their estimation of total outflow rates, *Engwall et al.* [2009a] assumed that the source was the polar cap region, simply defined as the area above 70° geomagnetic latitude.

Haaland et al. [2012b] also assumed the open polar cap as the primary source region for their estimations. They used a polar cap area given by an empirical model by

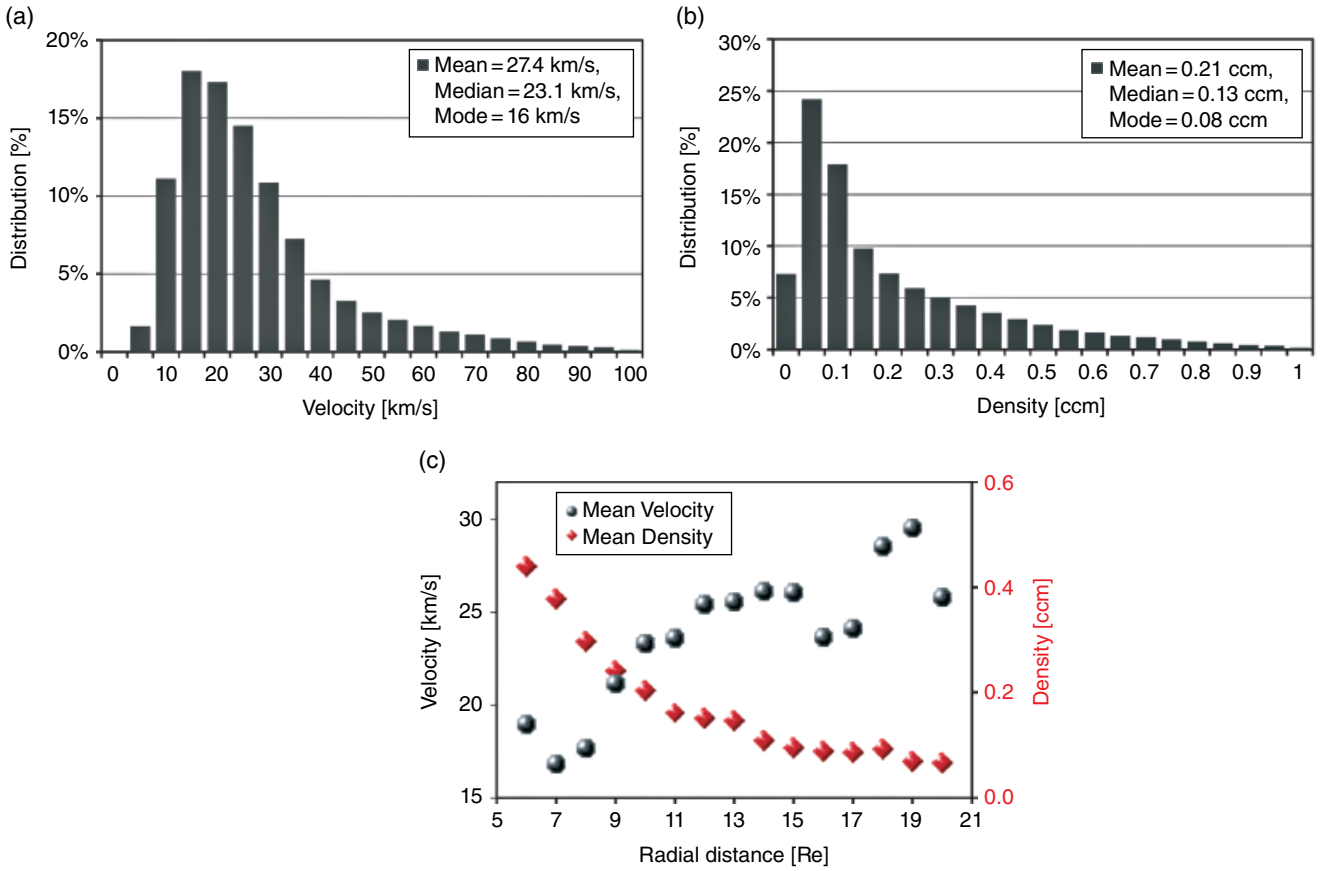

Figure 3.3 Panels a and b: Distribution of velocity and density, respectively. Panel c: Radial distance dependence of density (red color; values given by right vertical axis) and velocity (black color, left vertical axis).

Sotirelis et al. [1998]. This approach took into account that the polar cap region size can vary significantly with geomagnetic activity. For prolonged periods with northward interplanetary magnetic field (IMF) conditions, the polar cap area, and thus the source area of the polar wind can shrink to less than half than its average size.

An even more elaborate determination of the source area was undertaken by *Li et al.* [2012]. They used particle tracing [*Northrop and Scott*, 1964], taking all relevant forces into account, traced the ion transport path back to the ionosphere, and generated maps of the source regions for various disturbance levels and solar wind conditions. The overall results, reproduced in Figure 3.4, largely corroborated the *Haaland et al.* [2012b], findings in terms of source region and source area.

An interesting result of the *Li et al.* [2012] study was the identification of enhanced outflow from the cusp region and from the vicinity of the nightside auroral region. These regions are normally associated with ion outflow of more ions with higher energies, and also often with a larger abundance of heavier ions due to the additional acceleration potentials in these regions. One possible explanation for the cold outflow from these regions is enhanced production of secondary electrons due to impact ionization of the neutral atmosphere. These secondary electrons behave in much the same way as photoelectrons in enhancing the electric field as well as the electron temperature.

The apparent north-south asymmetry in Figure 3.4 is an artifact of the Cluster orbit. Southern hemisphere measurements are on average taken 1 R_E higher than in the northern hemisphere. Southern hemisphere data will therefore be biased toward data from the dayside/cusp region whereas northern hemisphere measurements will contain a larger fraction of ions that can be traced back to the nightside and the auroral region.

3.4.3. The Role of Solar Irradiance and the Solar Wind

Solar irradiance is the most important driver of ionization in the polar cap region. The $F_{10.7}$ index, a proxy for the total emission (in units of 10^{-2}Wsm^{-2}) from the solar disc at 10.7 cm wavelength, is frequently used to characterize solar irradiance. Figure 3.5 shows the in situ measured density and outflow velocity and the calculated

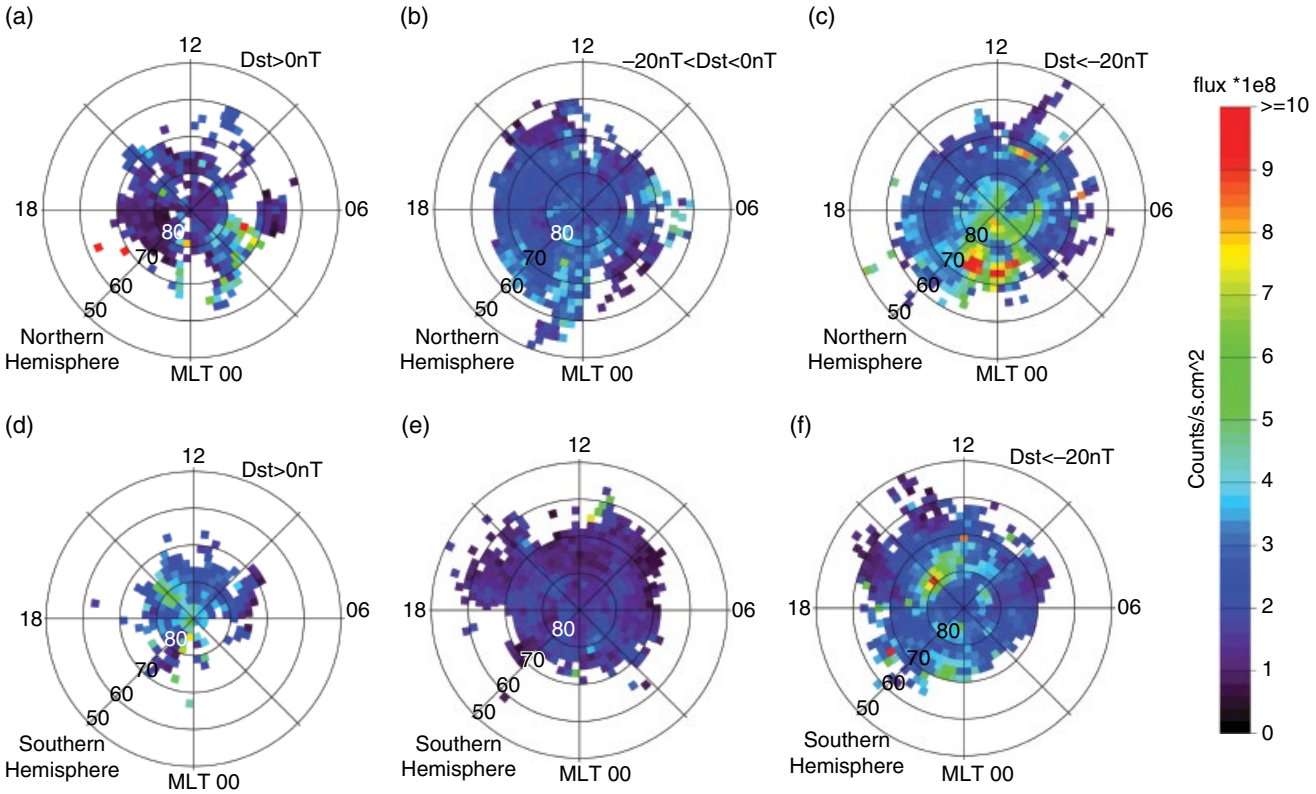

Figure 3.4 Maps of the source regions for cold ion outflow. Color indicates flux values. Panel a to c: Average ionospheric outflow fluxes in the northern hemisphere for quiet, moderate, and disturbed geomagnetic conditions. Panel d to e: Corresponding fluxes for southern hemisphere. After *Li et al.* [2012].

flux, mapped to 1000 km in the topside thermosphere, as a function of the $F_{10.7}$ index.

We note from Figure 3.5, which is essentially a reproduction of Figure 3.5 in *André et al.* [2014], that the outflow velocity does not seem to vary significantly with solar irradiance. All values in this binned distribution are in the range of 20 to 30 kms^{-1}, and there is no significant systematic increase in velocity with increasing solar activity. The density, however, varies more than a factor of 2 between low and high solar activity, consistent with the Cluster results reported in *Svenes et al.* [2008] and *Lybekk et al.* [2012]. The mapped flux also shows a marked increase with increasing solar activity.

In addition to the long time solar cycle variation of solar irradiance, there is also a seasonal and daily variation in the solar illumination. Since the Cluster orbit is only suitable for cold ion detection using the above methodology during the period around equinox, we are not able to address seasonal effects. Interestingly, the source maps shown in Figure 3.4 do not reveal any significant differences between the sunlit and the dark ionosphere in terms of mapped flux, although such a day/night asymmetry would be expected from models [e.g., *Glocer et al.*, 2012].

Solar wind-magnetosphere interaction, and in particular dayside reconnection, is a significant driver for magnetospheric circulation. Secondary effects of this interaction, in particular particle precipitation, is another significant mechanism for ionization, but is most prominent in the auroral zone and cusp regions and to a lesser degree in the open polar cap regions.

Some caution is necessary when interpreting the role of the solar wind dynamic pressure on ion outflow. An enhanced solar wind pressure leads to a compression of the whole magnetosphere. To the first order, this will be manifested as higher plasma density throughout the magnetosphere, but the actual supply of ionospheric material does not necessarily increase.

There are also other conceivable correlations of the cold ion flux. For example, the polar wind flux depends on the thermosphere neutral hydrogen density, which varies with solar cycle, as well as the O^+ density, which varies in response to a number of effects [e.g., *Yau et al.*, 2011].

In summary, however, results based on the Cluster cold ion data set suggest that solar illumination primarily controls ionization and outflow flux, whereas solar wind-magnetosphere interaction mainly affects transport.

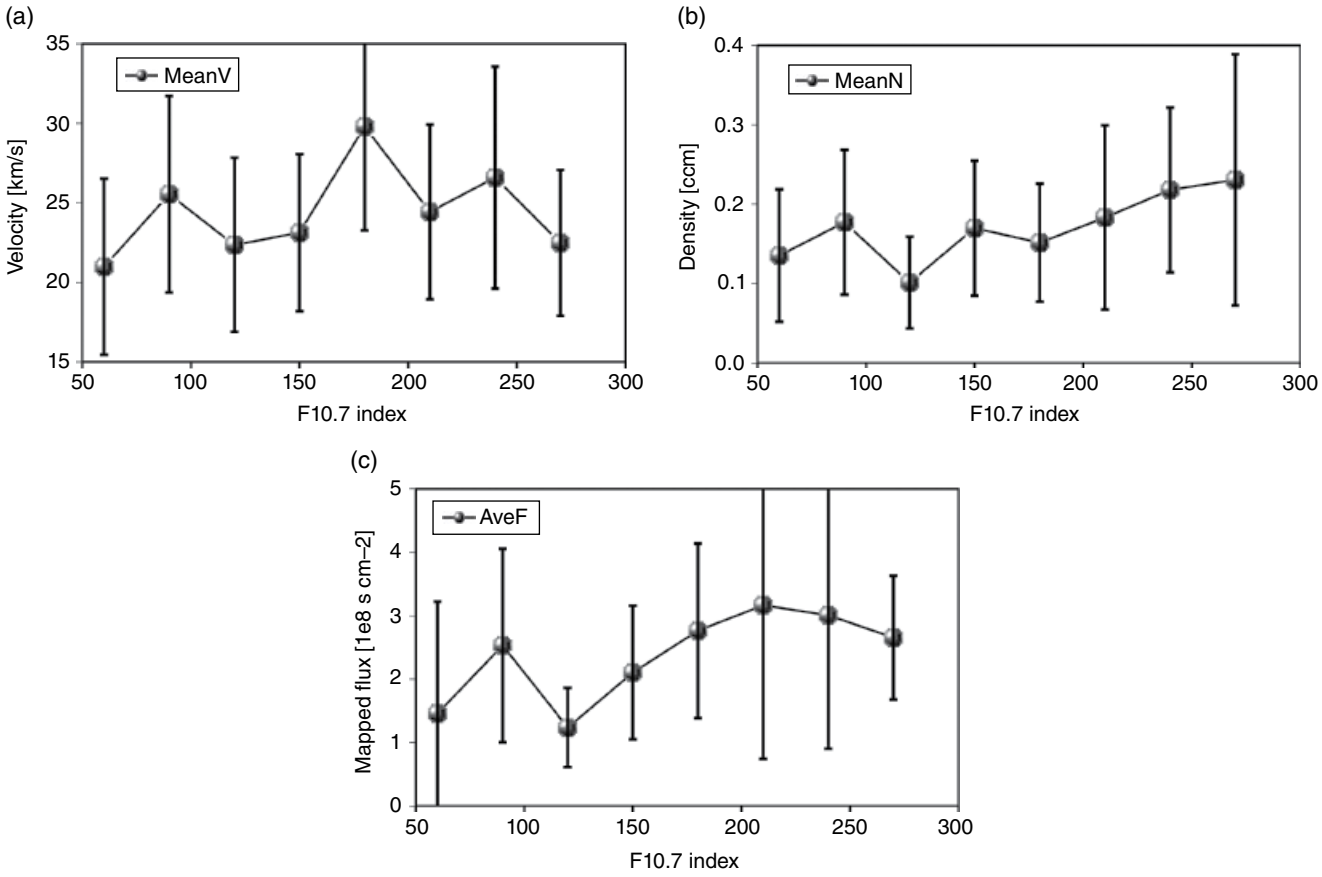

Figure 3.5 Panel a: In situ (e.g., measured at 4–19 Re) cold ion velocity (black) as function of solar irradiance as expressed by the $F_{10.7}$ index (see text for details). Panel b: Density as a function of solar irradiance. Panel c: Mapped flux as a function of solar irradiance. Error bars indicate statistical spread (standard deviation) of the measurements. [See also Figure 3.5 in *André et al.,* 2014].

The latter, and in particular the role of the IMF and convection, will be discussed further in the sections below.

3.4.4. Transport of Cold Ions to the Magnetosphere

The motion of the outflowing ions consists of a combination of parallel velocity and convection. Figure 3.6a schematically illustrates the motion of an individual ion from a given location in the ionosphere during moderately disturbed conditions with some convection.

At time t_1, the ion has escaped the Earth's gravitation potential and moves upward along an open field line (red lines in Figure 3.6a). At time t_2, the ion has moved further outward along the same field line, but this field line has now convected toward the plasma sheet, and will eventually be closed (i.e., reconnected in the tail) before the ion reaches the reconnection line. Thus, despite starting out on open field lines, this ion will be transported to the nightside plasma sheet where it contributes to plasma sheet refilling and plasma sheet dynamics.

From Figure 3.6a it is apparent that the initial position of the ion also plays a role. Ions escaping on from the dayside ionosphere and cusp region will be on field lines that will have to be convected a longer distance before reaching the plasma sheet. By the same token, ions escaping from the nightside ionosphere will have a shorter transport path to the magnetosphere. With parallel outflow velocities of the order of 20 to 30 kms^{-1}, the transport times from the ionospheric source to the nightside plasma sheet is in the order of several hours [see e.g., Table 1 in *Li et al.*, 2013].

Recent results from *Li et al.* [2016] indicates a region of stagnant outflow motion, and thus enhanced density near the high altitude dayside cusp region. These indications stem from the tracing results of *Li et al.* [2012], in which a number of tracing results suggested a parallel velocity close to zero in this region. The implications of this finding are not yet fully understood. One hypothesis is that the outward transport becomes stagnant in the transition region between the domain of the ambient

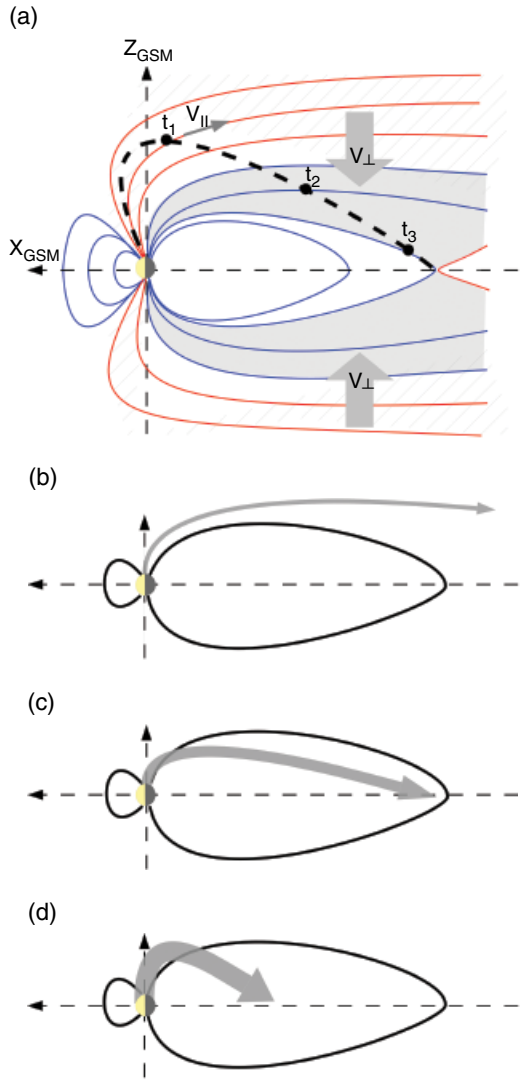

Figure 3.6 Panel a: Schematic trajectory of an individual ion from the ionosphere to the magnetosphere (dashed solid line). The motion consists of a field aligned and a convective part. If convection is sufficiently large compared to the parallel velocity, an ion initially on open field lines (t_1) will eventually be convected to the plasma sheet (t_3). Panel b to d: Effect of disturbance levels. For stagnant convection (panel a), the outflow is low and most ions escape on open field lines downtail. For intermediate geoactivity, there is more outflow but still slow convection. The ions are transported further tailward. During strong geomagnetic activity, the total outflow is higher, mainly due to the expanded polar cap area. The convection is also stronger, transporting more material to the near-Earth plasma sheet.

electric field responsible for extracting the ions in the first place, and a region at slightly higher altitudes where centrifugal acceleration becomes active. In this region, an equilibrium between upward and downward forces may be established under certain conditions. Unless there are any strong convection, cold ions would then pile up in this region.

3.4.4.1. Acceleration

The ambipolar electric field responsible for the extraction of the ions probably reach up to a few R_E altitudes [cf. the simulations by *Su*, 1998, mentioned above]. Above this, there is probably no significant electric field. However, due to centrifugal acceleration [e.g., *Cladis*, 1986], the ions will continue to increase their parallel velocity as they travel outward. The local acceleration is probably very small, but since it works over long distances, the total parallel velocity increase can be significant between the ionosphere and the far tail.

Nilsson et al. [2010] used data based on the wake method to quantify the acceleration due to centrifugal forces, and found averages local acceleration of the order of 5 ms^{-2}, which on average gave the ions an additional 5 to 10 km/s velocity over the 5 to 20 R_E range Cluster covers. Figure 3.3c, derived from the new complete data set seem to corroborate these numbers. Centrifugal acceleration becomes less effective further downtail, where the magnetic field becomes more stretched out.

3.4.4.2. Loss Versus Recirculation

Most of the low energy ion escape takes place on open magnetic field lines. However, as illustrated in Figure 3.6, it does not necessarily mean that these ions are lost into interplanetary space.

Haaland et al. [2012b] combined outflow velocities from *Engwall et al.* [2009a] with lobe convection results from *Haaland et al.* [2008] to estimate the loss versus circulation. They found that the largest direct downtail losses occurred under northward IMF conditions with stagnant convection. Except from effects of centrifugal acceleration discussed above, the field aligned velocity of the cold ions does not seem to vary significantly with IMF or geomagnetic disturbance. Convection, largely controlled by the dayside reconnection, on the other hand, is strongly dependent on IMF direction. Consequently, the transport of cold ions from the ionosphere into the magnetosphere is essentially controlled by convection, as illustrated in panels b, c, and d in Figure 3.6.

Table 3.1, compiled from Tables 2 and 3 in *Haaland et al.* [2012a], shows average velocities, densities, and fluxes for different IMF orientations and geomagnetic disturbance levels.

A more detailed study about the fate of the cold ions was conducted by *Li et al.* [2013]. As in the construction of the source maps shown in Figure 3.4, they used a full particle tracing of the measured outflow velocity and density, combined it with the measured convection and a model magnetic field [*Tsyganenko*, 2002] to estimate the

Table 3.1 Measured and calculated key parameters based on the cold ion data set of *Engwall et al.* [2009a]. We have divided the full dataset into subsets containing three different disturbance levels (first rows) and four different orientation of the interplanetary magnetic field (lower rows). This table is based on Tables 2 and 3 in *Haaland et al.* [2012b]. For each subset of disturbance levels and IMF directions, the different columns indicate the following: B: Average Dst.; C: Average IMF By value; D: Average IMF Bz value; E: Average plasma density; F: Average outflow velocity; G: Average mapped flux; H: Average convection velocity based on the *Haaland et al.* [2008] data set; I: Total outflow. (Based on the mapped flux [column G] and the polar cap arcs (estimated from *Sotirelis et al.* [1998]); J: Direct downtail loss, i.e., ions unable to convect to plasma sheet before passing distant X-line

A	B	C	D	E	F	G	H	I	J
	Averages taken from *Engwall et al.* [2009a]						Calculated values		
Activity/conditions	Dst	IMF By	IMF Bz	Ne	$V_{\|\|}$	Flux	$V_{\perp}$	Outflow	Loss
	[nT]	[nT]	[nT]	[cm]	[km s^{-1}]	[s^{-2} cm^{-1}]	[km s^{-2}]	[s^{-1}]	[$^{-1}$]
Quiet (Dst > 0 nT)	−43.0	1.4	−1.4	0.184	23.1	1.21e8	4.5	2.6e25	2.5e25
Moderate (−20 < Dst < 0)	−10.4	−0.5	−0.5	0.127	23.3	0.87e8	6.9	2.1e25	7.4e24
Storm (Dst < −20 nT)	7.5	−1.2	0.5	0.209	28.1	1.48e8	10.1	4.2e25	1.7e24
IMF By+	−29.8	4.6	0.0	0.172	25.8	1.22e8	8.0	2.6e25	1.0e24
IMF By −	−19.8	−5.4	−0.9	0.141	25.2	0.99e8	7.9	2.1e25	1.8e24
IMF Bz+	−39.2	−0.4	−4.6	0.196	24.6	1.35e8	1.7	1.1e25	7.2e24
IMF Bz −	−21.9	0.7	3.7	0.233	26.9	1.48e8	12.2	6.4e25	0

fate of the ions. Each individual observation was traced from the spacecraft position to a position slightly above the plasma sheet (no tracing was done inside the estimated plasma sheet, as the tracing assumptions break down here).

Figure 3.7 (based on Figures 5 and 6 in *Li et al.* [2013]) shows maps of the plasma sheet landing regions for the cold ions. During quiet and moderate conditions, the supply to the plasma sheet is typically below $10^5 s^{-1}$ (dark blue color) and spread out over a wide region. Some of the ions end up more than 60 R_E downtail. During disturbed conditions, fluxes are generally higher (green and red color, corresponding to fluxes above $10^5 s^{-1}$) and also deposited closer to Earth, with the majority of the deposition on between 20 to 30 R_E downtail.

Another interesting result from the *Li et al.* [2013] study, and also seen in Figure 3.7, is the dawn dusk asymmetry in the deposition. For disturbed conditions there seems to be a larger deposition on the duskside. The reason for this asymmetry is not fully clear, but external effects such as a bias in the interplanetary magnetic field can not fully explain the asymmetry [*Walsh et al.*, 2014a].

3.5. SUMMARY AND OUTLOOK

The unique combination of two complementary electric field techniques onboard the Cluster spacecraft and a novel technique has made it possible to estimate ion outflow velocities and densities of low energy ions. The novel technique is based on the detection of a wake forming of the positively charged spacecraft in a supersonic ion bulk flow region, and a functional dependence between the ambient plasma density and the spacecraft potential. The method is most sensitive to protons with energies up to a few tens of eV.

3.5.1. Summary of Experimental Results

The Cluster observations of cold plasma has provided us with new opportunities to study outflow and transport of cold ions from the ionosphere to the magnetosphere. In particular, it has been possible to quantify velocities, densities, and fluxes and their dependence on external drivers such as solar activity, solar wind-magnetosphere interaction, and geomagnetic activity.

The main experimental results from Cluster cold ion data set and studies thereof so far can be summarized in the following points:

- Typical field aligned outflow velocities measured in situ by Cluster in the high altitude polar cap and lobe regions (8–14 R_E altitude) are around 20 kms^{-1}. Typical plasma densities are around 0.1 cm^{-3}.
- Mapped to the ionosphere, the outflow rate is of the order of 1e-8 s^{-1}cm^{-2}. Integrated over the total polar cap area, the total outflow is of the order 1e26 s^{-1}.
- The outflow velocity is not very much affected by solar irradiance, but the density, and thus outflow rate vary almost a factor 3 between low solar irradiance and high irradiance.
- Outflow velocity or density do not vary significantly with geomagnetic activity or solar wind-magnetosphere interaction, but the convection and thus the fate of the

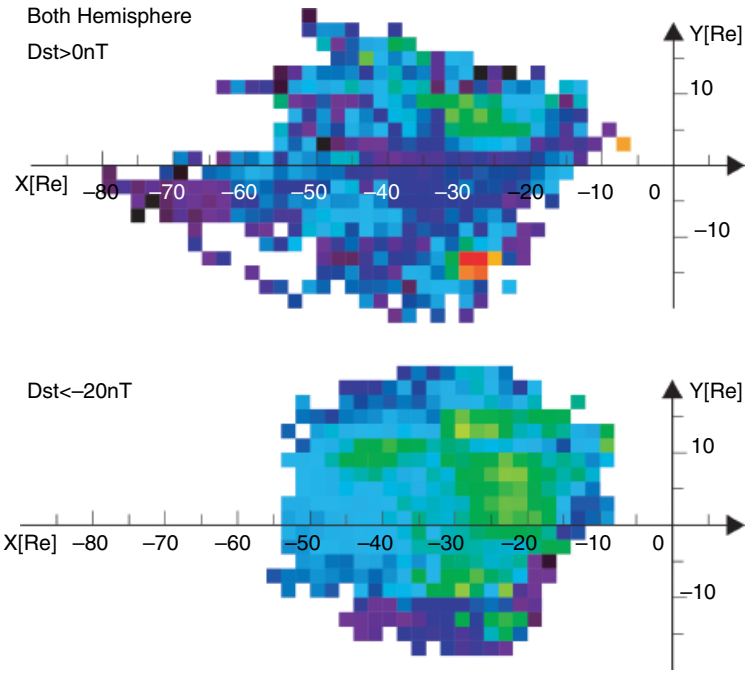

Figure 3.7 Maps of landing regions in the plasma sheet for the cold ions for quiet (top panel) and disturbed geomagnetic conditions. To construct these maps, individual ions from both hemispheres were mapped to a position slightly above the plasma sheet, and grouped into a 2x2 R_E bins. Colors indicate average fluxes within these bins. [Adapted from Figures 5 and 6 in *Li et al.*, 2013].

ions are strongly dependent on IMF direction and geomagnetic activity.

• Transport times from the ionosphere to the plasmasheet in the nightside magnetosphere is on the order of 2 to 4 hours. There seems to be a larger deposition in the duskside plasma sheet.

• The fate of the outflowing ions are largely controlled by the convection. Overall, only about 10%, or 1e25 s^{-1} cold ions are directly lost downtail. The rest are recirculated within the magnetosphere where they eventually contribute to the formation of the plasma sheet and ring current population.

• As pointed out by *André and Cully* [2012], low-energy ions typically dominate the density in large regions of the magnetosphere on the nightside and in the polar regions. These ions also often dominate in the dayside magnetosphere, and can alter the dynamics of processes like magnetic reconnection [e.g., *Walsh et al.*, 2014b; *Toledo-Redondo et al.*, 2015].

3.5.2. Outlook and Open Questions

At the time of writing, there are also ongoing projects to incorporate the Cluster cold ion dataset into polar wind models [see e.g., *Glocer*, 2017; *Welling*, 2017; and other papers of this volume] and to use the data to study specific intervals or phenomena [e.g., *Haaland et al.*, 2015; *Li et al.*, 2016].

Most of the studies discussed in the present paper are concerned with high latitude and lobe regions. But new results, for example from the dayside magnetopause [e.g., *Walsh et al.*, 2014b; *Toledo-Redondo et al.*, 2015; *Sonnerup et al.*, 2015], taking cold plasma into account, indicate that cold ions can play a significant role for fundamental plasma properties, and significantly alter the dynamics also in other regions of space.

The Cluster cold ion data set has also left a few puzzling questions that deserve some attention. These questions follow:

Cold ions in the cusp and auroral zone: The main source of the cold ions detected by Cluster seems to be the open polar cap. The mapping results of *Li et al.* [2012] revealed an interesting feature, though. As seen in Figure 3.4, there seems to be enhanced outflow from the cusp and auroral regions. The peak fluxes are almost an order of magnitude higher than the more homogeneous regions in the central polar cap area.

The conventional view is that additional energy in the form of Poynting flux and/or additional acceleration due to field aligned potential drops is available in these regions. The cusp and auroral zone is therefore known to be the source of various types of outflow [see e.g., reviews

by *Yau and André*, 1997; *André and Yau*, 1997], but typically at higher energies and at times with a significant fraction of oxygen. It is unclear whether the enhanced fluxes of cold ions is a result of higher ionization and thus a larger source reservoir, or whether the enhanced energy input also favors mechanisms enabling the cold ions to escape (e.g., the impact of enhanced production of secondary electrons discussed above).

Dawn-dusk asymmetries: *Li et al.* [2013] and *Walsh et al.* [2014a] noted a persistent dawn-dusk asymmetry in the deposition of cold ions to the plasma sheet (see also Figure 3.7). There seems to be an overall larger deposition on dusk. This asymmetry is not very apparent in the source maps (Figure 3.4) and may be a result of an overall dawn-dusk asymmetry in the transport between the ionosphere and magnetosphere rather than an inherent asymmetry in the polar cap source region. Modulation by IMF By cannot fully explain the asymmetry. A similar asymmetry was also noted by *Howarth and Yau* [2008] and *Yau et al.* [2012] in studies of oxygen outflow, but they related the asymmetry to IMF By effects during the transit from the ionosphere to the magnetosphere.

A stagnant region of cold ions in the high altitude dayside cusp/cleft region: In their attempts to trace the cold ions from the Cluster spacecraft to its source region, *Li et al.* [2012] noted that a significant fraction of the tracing result suggested zero parallel velocity around the high altitude dayside cusp/cleft region. Presently, no complete explanations for these stagnation regions exist [*Li et al.*, 2016].

ACKNOWLEDGMENTS

Work at the University of Bergen is supported by the Norwegian Research Council under grant 216872/F50 and the Fritjof Nansen Fund for Scientific Research. Computer code used for the calculations in this paper has been made available as part of the QSAS science analysis system. Solar wind data were obtained from the Coordinated Data Analysis Web (CDAWeb, see http://cdaweb.gsfc.nasa.gov/about.html). We also thank the International Space Science Institute, Bern, Switzerland, for providing computer resources and infrastructure for data exchange.

REFERENCES

Abe, T., B. A. Whalen, A. W. Yau, R. E. Horita, S. Watanabe, and E. Sagawa (1993), EXOS D (Akebono) suprathermal mass spectrometer observations of the polar wind, *J. Geophys. Res.*, *98*, 11,191, doi:10.1029/92JA01971.

André, M., and C. M. Cully (2012), Low-energy ions: A previously hidden solar system particle population, *Geophys. Res. Lett.*, *39*, L03101, doi:10.1029/2011GL050242.

André, M., and A. Yau (1997), Theories and Observations of Ion Energization and Outflow in the High Latitude Magnetosphere, *Space Sci. Rev*, *80*, 27–48, doi:10.1023/A:1004921619885.

André, M., K. Li, and A. Eriksson (2014), Outflow of low-energy ions and the solar cycle, *J. Geophys. Res.*, *33*, doi:10.1002/2014JA020714.

Axford, W. I. (1968), The Polar Wind and the Terrestrial Helium Budget, *J. Geophys. Res., 73*, 6855–6859, doi:10.1029/JA073i021p06855.

Banks, P. M., and T. E. Holzer (1968), The polar wind, *J. Geophys. Res.*, *73*(21), 6846–6854, doi:10.1029/JA073i021p06846.

Chandler, M. O., T. E. Moore, and J. H. Waite, Jr. (1991), Observations of polar ion outflows, *J. Geophys. Res.*, *96*, 1421–1428, doi:10.1029/90JA02180 .

Chappell, C. R., T. E. Moore, and J. H. Waite, Jr. (1987), The ionosphere as a fully adequate source of plasma for the earth's magnetosphere, *J. Geophys. Res.*, *92*, 5896–5910, doi:10.1029/JA092iA06p05896 .

Chappell, C. R., B. L. Giles, T. E. Moore, D. C. Delcourt, P. D. Craven, and M. O. Chandler (2000), The adequacy of the ionospheric source in supplying magnetospheric plasma, *Journal of Atmospheric and Solar-Terrestrial Physics*, *62*, 421–436, doi:10.1016/S1364-6826(00)00021-3.

Cladis, J. B. (1986), Parallel acceleration and transport of ions from polar ionosphere to plasma sheet, *Geophys. Res. Lett., 13*, 893–896, doi:10.1029/GL013i009p00893.

Dessler, A. J., and F. C. Michel (1966), Plasma in the geomagnetic tail, *J. Geophys. Res., 71*, 1421–1426, doi:10.1029/JZ071i005p01421.

Engwall, E., A. I. Eriksson, M. André, I. Dandouras, G. Paschmann, J. Quinn, and K. Torkar (2006), Low-energy (order 10 eV) ion flow in the magnetotail lobes inferred from spacecraft wake observations, *Geophys. Res. Lett.*, *33*, L06110, doi:10.1029/2005GL025179.

Engwall, E., A. I. Eriksson, C. M. Cully, M. André, P. A. Puhl-Quinn, H. Vaith, and R. Torbert (2009a), Survey of cold ionospheric outflows in the magnetotail, *Annales Geophysicae*, *27*, 3185–3201, doi:10.5194/angeo-27-3185-2009.

Engwall, E., A. I. Eriksson, C. M. Cully, M. André, R. Torbert, and H. Vaith (2009b), Earth's ionospheric outflow dominated by hidden cold plasma, *Nature Geoscience*, *2*, 24–27, doi:10.1038/ngeo387.

Escoubet, C. P., and R. Schmidt (2000), Cluster II: Plasma Measurements in Three Dimensions, *Advances in Space Research*, *25*, 1305–1314.

Escoubet, C. P., R. Schmidt, and M. L. Goldstein (1997), Cluster - Science and Mission Overview, *Space Sci. Rev*, *79*, 11–32, doi:10.1023/A:1004923124586.

Glocer, A. (2015), *Coupling Ionospheric outflow to magnetospheric models*, chap. 15, p. 195, this volume, AGU Geophysical Monograph Series, Wiley.

Glocer, A., N. Kitamura, G. Toth, and T. Gombosi (2012), Modeling solar zenith angle effects on the polar wind, *J. Geophys. Res.*, *117*, A04318, doi:10.1029/2011JA017136.

Gustafsson, G., M. André, T. Carozzi, A. I. Eriksson, C. G. Fälthammar, R. Grard, G. Holmgren, J. A. Holtet, N. Ivchenko, T. Karlsson, Y. Khotyaintsev, S. Klimov, H. Laakso, P. A. Lindqvist, B. Lybekk, G. Marklund,

F. S. Mozer, K. Mursula, A. Pedersen, B. Popielawska, S. Savin, K. Staziewicz, P. Tanskanen, A. Vaivads, and J. E. Wahlund (2001), First results of electric field and density measurements by Cluster EFW based on initial months of operation, *Annales Geophysicae*, *19*, 1219.

Haaland, S., G. Paschmann, M. Förster, J. Quinn, R. Torbert, H. Vaith, P. Puhl-Quinn, and C. Kletzing (2008), Plasma convection in the magnetotail lobes: statistical results from Cluster EDI measurements, *Annales Geophysicae*, *26*, 2371–2382, doi:10.5194/angeo-26-2371-2008.

Haaland, S., A. Eriksson, E. Engwall, B. Lybekk, H. Nilsson, A. Pedersen, K. Svenes, M. André, M. Förster, K. Li, C. Johnsen, and N. Østgaard (2012a), Estimating the capture and loss of cold plasma from ionospheric outflow, *J. Geophys. Res.*, *117*, A07311, doi:10.1029/2012JA017679.

Haaland, S., K. Svenes, B. Lybekk, and A. Pedersen (2012b), A survey of the polar cap density based on Cluster EFW probe measurements: Solar wind and solar irradiation dependence, *J. Geophys. Res.*, *117*, A01216, doi:10.1029/2011JA017250.

Haaland, S., A. Erikson, L. Maes, M. André, L. Baddeley, A. Barakat, R. Chappell, V. Eccles, C. Johnsen, K. Li, B. Lybekk, A. Pedersen, R. Schunk, and D. Welling (2015), Estimation of cold plasma outflow during geomagnetic storms, *J. Geophys. Res.,* p. in review.

Hoffman, J. H. (1970), Studies of the composition of the ionosphere with a magnetic deflection mass spectrometer, Int. J. Mass Spectrom. Ion Phys, pp. 315–322, doi:10.1016/0020-7381(70)85047-1.

Hoffman, J. H., W. H. Dodson, C. R. Lippincott, and H. D. Hammack (1974), Initial ion composition results from the Isis 2 satellite, *J. Geophys. Res.*, *79*, 4246–4251, doi:10.1029/JA079i028p04246.

Horwitz, J. L. (1982), The ionosphere as a source for magnetospheric ions, *Reviews of Geophysics and Space Physics*, *20*, 929–952, doi:10.1029/RG020i004p00929.

Howarth, A., and A. W. Yau (2008), The effects of IMF and convection on thermal ion outflow in magnetosphere-ionosphere coupling, *Journal of Atmospheric and Solar-Terrestrial Physics*, *70*, 2132–2143, doi:10.1016/j.jastp.2008.08.008.

Kitamura, N., K. Seki, and Y. Nishimura (2015), *Thermal and low-energy outflows in an through the polar cap*, chap. 7, p. 91, this volume, AGU Geophysical Monograph Series, Wiley.

Li, K., S. Haaland, A. Eriksson, M. André, E. Engwall, Y. Wei, E. A. Kronberg, M. Fränz, P. W. Daly, H. Zhao, and Q. Y. Ren (2012), On the ionospheric source region of cold ion outflow, *Geophys. Res. Lett.*, *39*, L18102, doi:10.1029/2012GL053297 .

Li, K., S. Haaland, A. Eriksson, M. André, E. Engwall, Y. Wei, E. A. Kronberg, M. Fränz, P. W. Daly, H. Zhao, and Q. Y. Ren (2013), Transport of cold ions from the polar ionosphere to the plasma sheet, *J. Geophys. Res.*, *118*, 5467–5477, doi:10.1002/jgra.50518.

Li, K., S. Haaland, P. W. Daly, E. A. Kronberg, M. André, A. Eriksson, A. Pedersen, B. Lybekk, and Y. Wei (2016), On the dayside high altitude stagnant region of cold ion outflow, *J. Geophys. Res.*, *120*, in review.

Lockwood, M., J. H. Waite, Jr., T. E. Moore, C. R. Chappell, and J. F. E. Johnson (1985a), A new source of suprathermal O(+) ions near the dayside polar cap boundary, *J. Geophys. Res., 90*, 4099–4116, doi:10.1029/JA090iA05p04099.

Lockwood, M., J. H. Waite, Jr., T. E. Moore, C. R. Chappell, and M. O. Chandler (1985b), The cleft ion fountain, *J. Geophys. Res.*, *90*, 9736–9748, doi:10.1029/JA090iA10p09736.

Lybekk, B., A. Pedersen, S. Haaland, K. Svenes, A. N. Fazakerley, A. Masson, M. G. G. T. Taylor, and J.-G. Trotignon (2012), Solar cycle variations of the Cluster spacecraft potential and its use for electron density estimations, *J. Geophys. Res.*, *117*, A01217, doi:10.1029/2011JA016969.

Nilsson, H., E. Engwall, A. Eriksson, P. A. Puhl-Quinn, and S. Arvelius (2010), Centrifugal acceleration in the magnetotail lobes, *Annales Geophysicae*, *28*, 569–576, doi:10.5194/angeo-28-569-2010.

Northrop, T. G., and F. R. Scott (1964), The Adiabatic Motion of Charged Particles, *American Journal of Physics*, *32*, 807–807, doi:10.1119/1.1969867.

Olsen, R. C. (1982), The hidden ion population of the magnetosphere, *J. Geophys. Res., 87*, 3481–3488, doi:10.1029/JA087iA05p03481.

Olsen, R. C., C. R. Chappell, D. L. Gallagher, J. L. Green, and D. A. Gurnett (1985), The hidden ion population, Revisited, *J. Geophys. Res.*, *90*, 12,121, doi:10.1029/JA090iA12p12121.

Paschmann, G., F. Melzner, R. Frenzel, H. Vaith, P. Parigger, U. Pagel, O. H. Bauer, G. Haerendel, W. Baumjohann, N. Scopke, R. B. Torbert, B. Briggs, J. Chan, K. Lynch, K. Morey, J. M. Quinn, D. Simpson, C. Young, C. E. McIlwain, W. Fillius, S. S. Kerr, R. Mahieu, and E. C. Whipple (1997), The Electron Drift Instrument for Cluster, *Space Sci. Rev*, *79*, 233–269.

Pedersen, A., P. Décréau, C. Escoubet, G. Gustafsson, H. Laakso, P. Lindqvist, B. Lybekk, A. Masson, F. Mozer, and A. Vaivads (2001), Four-point high time resolution information on electron densities by the electric field experiments (EFW) on Cluster, *Ann. Geophys.*, *19*, 1483–1489, doi:10.5194/angeo-19-1483-2001.

Quinn, J. M., G. Paschmann, R. B. Torbert, H. Vaith, C. E. McIlwain, G. Haerendel, O. Bauer, T. M. Bauer, W. Baumjohann, W. Fillius, M. Foerster, S. Frey, E. Georgescu, S. S. Kerr, C. A. Kletzing, H. Matsui, P. Puhl-Quinn, and E. C. Whipple (2001), Cluster EDI convection measurements across the high-latitude plasma sheet boundary at midnight, *Ann. Geophys.*, *19*, 1669–1681.

Riedler, W., K. Torkar, F. Rudenauer, M. Fehringer, A. Pedersen, R. Schmidt, R. J. L. Grard, H. Arends, B. T. Narheim, J. Troim, R. Torbert, R. C. Olsen, E. Whipple, R. Goldstein, N. Valavanoglou, and H. Zhao (1997), Active Spacecraft Potential Control, *Space Sci. Rev*, *79*, 271–302, doi:10.1023/A:1004921614592.

Sonnerup, B., G. Paschmann, S. Haaland, T. Phan, and S. Eriksson (2015), Reconnection layer bounded by switch-off shocks: Magnetopause crossing by themis d on 03 august 2008, *J. Geophys. Res., 121*, 3310–3332, doi:10.1002/2016JA022362.

Sotirelis, T., P. T. Newell, and C. Meng (1998), Shape of the open-closed boundary of the polar cap as determined from observations of precipitating particles by up to four DMSP satellites, *J. Geophys. Res.*, *103*, 399–406, doi:10.1029/97JA02437.

Su, Y.-J. (1998), The photoelectron-driven polar wind: Coupled fluid- semikinetic simulations and measurements by the

thermal ion dynamics experiment on the POLAR spacecraft, Ph.D. thesis, University of Alabama in Huntsville.

Su, Y.-J., J. L. Horwitz, T. E. Moore, B. L. Giles, M. O. Chandler, P. D. Craven, M. Hirahara, and C. J. Pollock (1998), Polar wind survey with the Thermal Ion Dynamics Experiment/Plasma Source Instrument suite aboard POLAR, *J. Geophys. Res.*, *103*, 29, 305–329, 338, doi:10.1029/98JA02662.

Svenes, K. R., B. Lybekk, A. Pedersen, and S. Haaland (2008), Cluster observations of near-Earth magnetospheric lobe plasma densities a statistical study, *Annales Geophysicae*, *26*, 2845–2852, doi:10.5194/angeo-26-2845-2008.

Toledo-Redondo, S., A. Vaivads, M. André, and Y. V. Khotyaintsev (2015), Modification of the Hall physics in magnetic reconnection due to cold ions at the Earth's magnetopause, *Geophys. Res. Lett., 42*, 6146–6154, doi:10.1002/2015GL065129.

Torkar, K., and H. Jeszenszky (2010), *ASPOC Data Products in the Cluster Active Archive*, pp. 39–49.

Tsyganenko, N. A. (2002), A model of the near magnetosphere with a dawn-dusk asymmetry 1. Mathematical structure, *J. Geophys. Res.*, *107*, 1179, doi:10.1029/2001JA000219.

Walsh, A. P., S. Haaland, C. Forsyth, A. M. Keesee, J. Kissinger, K. Li, A. Runov, J. Soucek, B. M. Walsh, S. Wing, and M. G. G. T. Taylor (2014a), Dawn-dusk asymmetries in the coupled solar wind-magnetosphere-ionosphere system: a review, *Annales Geophysicae*, *32*, 705–737, doi:10.5194/angeo-32-705-2014.

Walsh, B. M., T. D. Phan, D. G. Sibeck, and V. M. Souza (2014b), The plasmaspheric plume and magnetopause reconnection, *Geophys. Res. Lett.*, *41*, 223–228, doi:10.1002/2013GL058802.

Welling, D. T. (2015), *Recent advances in magnetosphere mass coupling in global models*, chap. 14, p. 179, AGU Geophysical Monograph Series, Wiley.

Whipple, E. C., J. M. Warnock, and R. H. Winkler (1974), Effect of satellite potential on direct ion density measurements through the plasmapause, *J. Geophys. Res.*, *79*, 179–186, doi:10.1029/JA079i001p00179.

Yau, A., W. K. Peterson, and T. Abe (2011), *Influences of the Ionosphere, Thermosphere and Magnetosphere on Ion Outflows*, chap. 3, pp. 283–314, IAGA Special Sopron Book Series, Springer Netherlands, doi:10.1007/978-94-007-0501-2-16.

Yau, A., W. K. Peterson, and T. Abe (2015), *Measurements of ion outflow from the Earth's ionosphere*, chap. 2, p. 21, this volume, AGU Geophysical Monograph Series, Wiley.

Yau, A. W., and M. André (1997), Sources of Ion Outflow in the High Latitude Ionosphere, *Space Sci. Rev*, *80*, 1–25, doi:10.1023/A:1004947203046.

Yau, A. W., A. Howarth, W. K. Peterson, and T. Abe (2012), Transport of thermal-energy ionospheric oxygen (O^+) ions between the ionosphere and the plasma sheet and ring current at quiet times preceding magnetic storms, *J. Geophys. Res.*, *117*, A07215, doi:10.1029/2012JA017803.